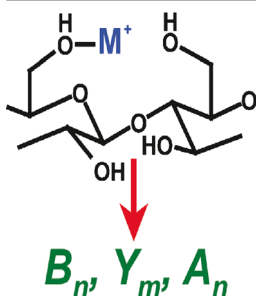


# Cationized Carbohydrate Gas-Phase Fragmentation Chemistry

Benjamin J. Bythell, Maha T. Abutokaikah, Ashley R. Wagoner, Shanshan Guan, Jordan M. Rabus

Department of Chemistry and Biochemistry, University of Missouri, St. Louis, MO 63121, USA



**Abstract.** We investigate the fragmentation chemistry of cationized carbohydrates using a combination of tandem mass spectrometry, regioselective labeling, and computational methods. Our model system is D-lactose. Barriers to the fundamental glycosidic bond cleavage reactions, neutral loss pathways, and structurally informative cross-ring cleavages are investigated. The most energetically favorable conformations of cationized D-lactose were found to be similar. In agreement with the literature, larger group I cations result in structures with increased cation coordination number which require greater collision energy to dissociate. In contrast with earlier proposals, the  $B_n$ - $Y_m$  fragmentation pathways of both protonated and sodium-cationized analytes proceed via protonation of the glycosidic oxygen with concerted glycosidic

bond cleavage. Additionally, for the sodiated congeners our calculations support sodiated 1,6-anhydrogalactose  $B_n$  ion structures, unlike the preceding literature. This affects the subsequent propensity of formation and prediction of  $B_n/Y_m$  branching ratio. The nature of the anomeric center ( $\alpha/\beta$ ) affects the relative energies of these processes, but not the overall ranking. Low-energy cross-ring cleavages are observed for the metal-cationized analytes with a retro-aldol mechanism producing the  $^{o,2}A_2$  ion from the sodiated forms. Theory and experiment support the importance of consecutive fragmentation processes, particularly for the protonated congeners at higher collision energies.

**Keywords:** Mass spectrometry, Collision-induced dissociation, Ion structure, Labeling, Metals, Density functional theory, Glycans

Received: 22 August 2016/Revised: 13 October 2016/Accepted: 14 October 2016/Published Online: 28 November 2016

## Introduction

Complex carbohydrates (glycans) are extremely important in chemistry and biology [1–3]. In addition to being a primary source of energy, they provide critical roles in intracellular signaling, recognition, immune response, homeostasis, as well as many disease states, vaccines, and therapeutics [1, 4–8]. In biological systems, glycans exist either as ‘free’ polysaccharides or more complicated mucosubstances such as glycoproteins, glycolipids, and mucins. Despite the multifaceted structures potentially formed, glycans are assembled from relatively simple components (hexose, pentose sugars), which are joined through

glycosylation reactions that generate glycosidic bonds (Figure 1). Depending on the specific physiological need/use, these may be chemically modified further.

Mass spectrometry (MS) has proven to be a powerful tool in many aspects of glycan analysis [4, 10–27]. Mass spectrometry coupled to a variety of fragmentation methods is utilized in glycan sequencing and glyco-proteomics. Ideally, individual analytes are isolated prior to activation, fragmentation, and detection (tandem MS or MS/MS). Identification of the sequence is subsequently attempted based on the detected mass-to-charge ( $m/z$ ) ratios corresponding to the charged fragments and the precursor ion. For a polysaccharide of length  $N = n + m$ , cleavage of the glycosidic bonds produces a series of  $B_n$  and/or  $C_n$  ions if the non-reducing end fragment keeps a charge (left-hand side in Figure 1 [9]), and/or  $Y_m$  and  $Z_m$  ions if the reducing end fragment keeps a charge (right-hand side in Figure 1), or a mixture of these fragments. Cross-ring cleavages ( $A_n$  and  $X_m$  ions) are also possible. These cross-ring cleavage ions are particularly

**Electronic supplementary material** The online version of this article (doi:10.1007/s13361-016-1530-x) contains supplementary material, which is available to authorized users.

Correspondence to: Benjamin J. Bythell; e-mail: bythellb@umsl.edu

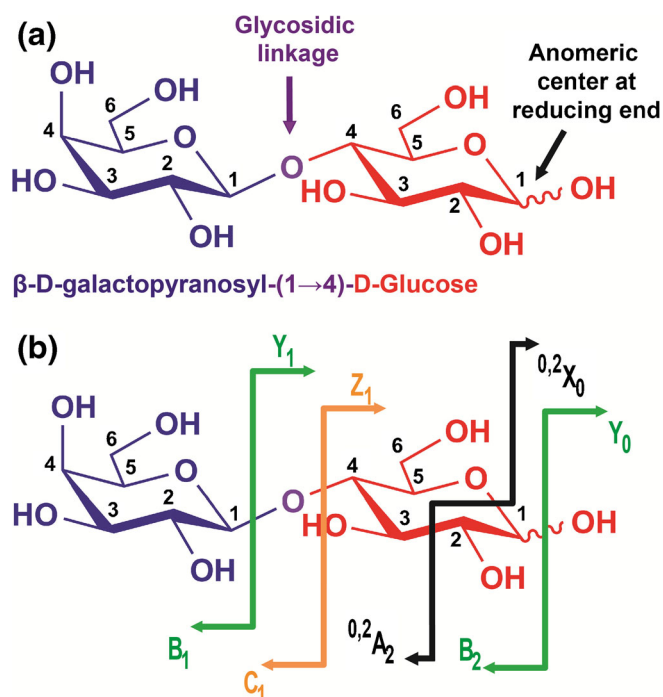


**Figure 1.** (a) Polysaccharide components, bonding, stereochemistry, and nomenclature illustrated for our model system, lactose:  $\beta$ -D-galactopyranosyl-(1 $\rightarrow$ 4)-D-glucose. (b) The carbohydrate fragmentation nomenclature of Domon and Costello [9] illustrated with our model system

important for glycans as they provide additional structural information, which potentially enables differentiation of isomers (Figure 1).

Unlike other biopolymers (peptides, nucleic acids), carbohydrates have multiple potential sites of propagation, generating enormous numbers of potentially relevant stereoisomers and multiple bonding arrangements (linear versus branched, coupled with stereochemistry at each glycosidic linkage site). Nature executes these propagation reactions efficiently to yield complex glycans tailored to an enormous variety of functions. Unfortunately, despite much progress in this area, synthesis of the standard compounds necessary for mass spectral libraries is fraught with difficulty. This means that there is a significant need for improved and/or complementary methods of identification for glycans. Recent advances in ion mobility MS have shown promise, enabling discrimination between isomers for some glycans [28–34]. Separation of identical elemental composition glycans prior to fragmentation is highly desirable, but still requires practical means of accurately interpreting the subsequent MS/MS spectra for each isomer. Thus, an improved understanding of the factors that govern glycan fragmentation as a function of analyte class, charging agent, and/or fragmentation method can potentially be leveraged to provide additional confidence in assignment of glycan sequences and glycosidic bonding motifs.

In the current article, we present our initial results in examining the mechanisms and energetics of polysaccharide fragmentation using a combination of isotopically labeled

substrates, tandem mass spectrometry, and computational methods. We utilize the common disaccharide lactose ( $\beta$ -D-galactopyranosyl-(1 $\rightarrow$ 4)-D-glucose) as our initial, ‘simple’ model system, cationized with a proton or with group I metals, as are commonly utilized in sugar sequencing [15, 16, 35]. We compare our experimental findings to the pre-existing literature [17, 22, 35–38] and make structural and energetic predictions based on our combined findings.

## Experimental

Experimental work was carried out using a MaXis plus electrospray-quadrupole time-of-flight mass spectrometer (Bruker, Billerica, MA, USA). The product ion mass spectra for  $[\text{lactose} + \text{M}]^+$  ions were obtained by mass-selecting the appropriate ion with the quadrupole, CID in the collision cell, followed by product dispersion by the time-of-flight analyzer ( $\text{M} = \text{H}^+, \text{Li}^+, \text{Na}^+$ ). Data were collected as a function of collision energy. Specific investigation of individual fragment ion types involved pseudo- $\text{MS}^3$  experiments. In this approach, in-source CID is achieved by adjustment of the potential difference between the two ion funnels located at the front of the instrument. Fragment ions generated in this process are then selected by the quadrupole mass filter for CID and mass analysis in the usual fashion. Breakdown graphs expressing the relative fragment ion signals as a function of collision energy were obtained for all species studied.

Ionization was by electrospray with the lactose samples infused into the instrument in  $\sim 5 \mu\text{M}$  acetonitrile/water/formic acid (50/50/0.1%) solutions at a flow rate of  $3 \mu\text{L min}^{-1}$ . Nitrogen was used as nebulizing, drying, and collision gas. Lactose ( $\beta$ -D-galactopyranosyl-(1 $\rightarrow$ 4)-D- $^{13}\text{C}_1$ -glucose) was purchased from Omicron Biochemicals, Inc. (South Bend, IN, USA). Regioselectively  $^{13}\text{C}$ -labeled lactose samples ( $\beta$ -D-galactopyranosyl-(1 $\rightarrow$ 4)-D- $^{13}\text{C}_6$ -glucose) were purchased from Cambridge Isotope Laboratories, Inc. (Tewksbury, MA, USA). Lithium chloride was purchased from Sigma-Aldrich (St. Louis, MO, USA). Lithium chloride at  $10 \mu\text{M}$  was utilized to provide lithiated precursor ions. No addition of sodium cations was necessary due to impurities in the dried lactose sample. For the deuterated labeling experiments [17], lactose was dissolved in  $\text{D}_2\text{O}$  for 10 min at room temperature, and the solution was further diluted in acetonitrile/ $\text{D}_2\text{O}$  (50/50%) to the final concentration of  $\sim 0.1 \text{ mM}$ . Deuterium oxide was purchased from Cambridge Isotope Laboratories, Inc (Tewksbury, MA, USA).

## Theoretical Methods

Density functional calculations of minima, as well as product ions and neutrals were performed with the Gaussian 09 suite of programs [39]. The M06-2X level of theory [40, 41] was utilized terminating with the 6-31+G(d,p) basis set. Multiple conformers of each protonation/cationization site were examined for each system type ( $\text{H}^+, \text{Li}^+, \text{Na}^+, \text{K}^+$ ). Initially we also examined conformers calculated with a much larger basis set

[6-311++G(2d,p)] and also the B3LYP functional to provide an estimate of whether large changes in structure or energetics were likely. Consistent with our prior work on peptide systems [42, 43], the structures were essentially identical and only small differences (typically  $<5$  kJ mol<sup>-1</sup>) in relative energy were identified. Consequently, we limited the subsequent calculations to the M06-2X/6-31+G(d,p) to avoid duplication of effort and reduce computational expense. Essentially, we want to use the smallest basis set that will accurately reproduce/predict the experimental data, so that we can investigate the largest, most widely interesting systems possible (i.e., so that larger, more biologically-interesting glycans can be studied computationally in the future). As an additional check of this approach, we also performed targeted single point calculations at multiple levels of theory (M06-2X, B3LYP, and MP2) on select critical precursor ion and transition structures to assess variability in the description of the chemistry.

We investigated the fragmentation pathways of the protonated and sodiated forms. Multiple transition structures (TSs) were calculated for each potential pathway. Minima were confirmed by vibrational analysis (all real frequencies) and TSs were also examined in this manner (one imaginary frequency). The reaction pathway through each TS was determined by intrinsic reaction coordinate (IRC) calculations with up to 10 steps in each direction. The terminating points of these calculations (one on product-side, one on reactant-side) were then optimized further to determine the exact minima connected by each specific reaction path. Estimates of the proton (metal) affinities of the leaving groups were determined as the difference between the zero-point energy-corrected M06-2X/6-31+G(d,p) total electronic energies (0 K) of the protonated and neutral forms of the potential sequence ion structures, respectively.

## Results and Discussion

### Experimental Findings

Our experimental data point to a shift in the propensities of the various fragmentation reactions possible with low-energy collisional activation as a function of choice of group 1 cation. This is consistent with the prevailing literature [16, 17, 28, 35]. Briefly, the protonated lactose fragments primarily via a combination of water-loss and glycosidic bond cleavages (Figure 2). There is no evidence of cross-ring cleavages. Our labeling data (Figure 2b and c) indicates that the nominal  $m/z$  163 peak is a mixture of fragments from both the reducing ( $Z_I$  and/or  $Y_I^{-H_2O}$ ) and non-reducing ends ( $B_I$ ). The  $m/z$  163 peak is split into a doublet (Figure 2b and c) indicating that the regioselective <sup>13</sup>C-labeled reducing end provides a substantial contribution to the detected ion current. The much lower abundance  $m/z$  145 peak also shows evidence of contributions from both the  $\beta$ -D-galactopyranosyl ( $m/z$  145 peak, Figure 2b and c) and glucose ends of the molecule (peaks at  $m/z$  146 and 151 in Figure 2b and c, respectively). This is consistent with either loss of water from the  $m/z$  163 species or consecutive formation from the abundant [lactose + H-H<sub>2</sub>O]<sup>+</sup> ions. In contrast, the more

abundant peak at  $m/z$  181 appears to be a  $Y_I$  ion as it shows no splitting with isotopic substitution. The  $m/z$  value shifts by an amount equal to the number of <sup>13</sup>C atoms present in the glucose residue (1 or 6, Figure 2b and c).

The lithium cationized precursors also show the  $B_I/Z_I/Y_I^{-H_2O}$  isotopomer peak ( $m/z$  169, Figure 3a) with the associated  $m/z$  shifts (1 or 6 u) based on the number of <sup>13</sup>C atoms present in the  $Z_I$  ions (Figure 3b and c). Unlike the situation for either the protonated or sodiated congeners, we also detect evidence of both reducing and non-reducing end fragments ( $Y_I$  and  $C_I$ ) at  $m/z$  187 (Figure 3b and c). This differs from the findings of Hofmeister et al. for [gentiobiose+Li]<sup>+</sup>, which indicated that there was only one glycosidic bond cleavage position leading exclusively to  $B_I$  and  $Y_I$  peaks [17]. This illustrates that disaccharide dissociation chemistry varies with analyte structure as gentiobiose and lactose are isomers that both contain  $\beta$  linkages to D-glucose at the reducing end. However, the gentiobiose linkage is 1 $\rightarrow$ 6 rather than 1 $\rightarrow$ 4, which imposes different structural constraints, as does the presence of D-glucose rather than D-galactose at the non-reducing end. Other differences relative to the protonated form observed are: (1) a substantial reduction in the relative propensity of water loss from the [lactose + Li]<sup>+</sup> precursor ion; (2) a peak at  $m/z$  205 corresponding to a reducing end (glucose) containing structure. Pseudo-MS<sup>3</sup> of this  $m/z$  provides data that is very similar to the corresponding  $Y_I$  ion supporting both the  $Y_I + H_2O$  assignment and that this is likely to be a water adduct [44]; (3) the presence of a cross-ring cleavage peak at  $m/z$  289 (<sup>0,2</sup> $A_2$  ion, Figures 1 and 3a). By combining our accurate mass and labeling data (Figure 3b and c), we have assigned this as a loss of C<sub>2</sub>H<sub>4</sub>O<sub>2</sub> (rather than the structurally unlikely loss of CO<sub>3</sub>) consistent with the literature [17]. Our labeling indicates this comes from the glucose end and that the neutral loss must include the anomeric carbon (carbon 1, Figure 1). Logically, this peak is thus assigned as <sup>0,2</sup> $A_2$  with the superscript indicating the cleavages between the glucose ring oxygen and the anomeric carbon, and after carbon 2 (Figure 1b). At higher collision energies (data not shown) we detect evidence of <sup>2,4</sup> $A_2$  ions as well ( $m/z$  229; loss of a further C<sub>2</sub>H<sub>4</sub>O<sub>2</sub>).

In contrast, the tandem mass spectrometry of the sodium cationized form is much simpler than the lithiated and protonated congeners. While the water loss peak remains, the  $m/z$  185 peak is formed from the non-reducing  $\beta$ -D-galactopyranosyl end of the analyte, so corresponds to the  $B_I$  ion. Similarly, the  $m/z$  203 peak shifts by an  $m/z$  amount equal to the additional mass of the isotopically labeled glucose residue (Figure 4b and c), so is provisionally assigned as  $Y_I$ . We also see clear evidence of a <sup>0,2</sup> $A_2$  peak at  $m/z$  305 (Figure 4a), again with a <sup>2,4</sup> $A_2$  peak ( $m/z$  245) at higher collision energy. In fact, the cross-ring cleavage <sup>0,2</sup> $A_2$  peak is more abundant than the glycosidic bond cleavages (Figure 4a) indicating a substantial change in relative favorability of the fragmentation chemistries.

More generally, we observe a substantial shift in the collision energies necessary to achieve a given level of precursor ion decomposition as the cation size increases. This again is consistent with the prevailing literature. Early work by the Lebrilla group identified this trend [15, 35, 45] and argued for

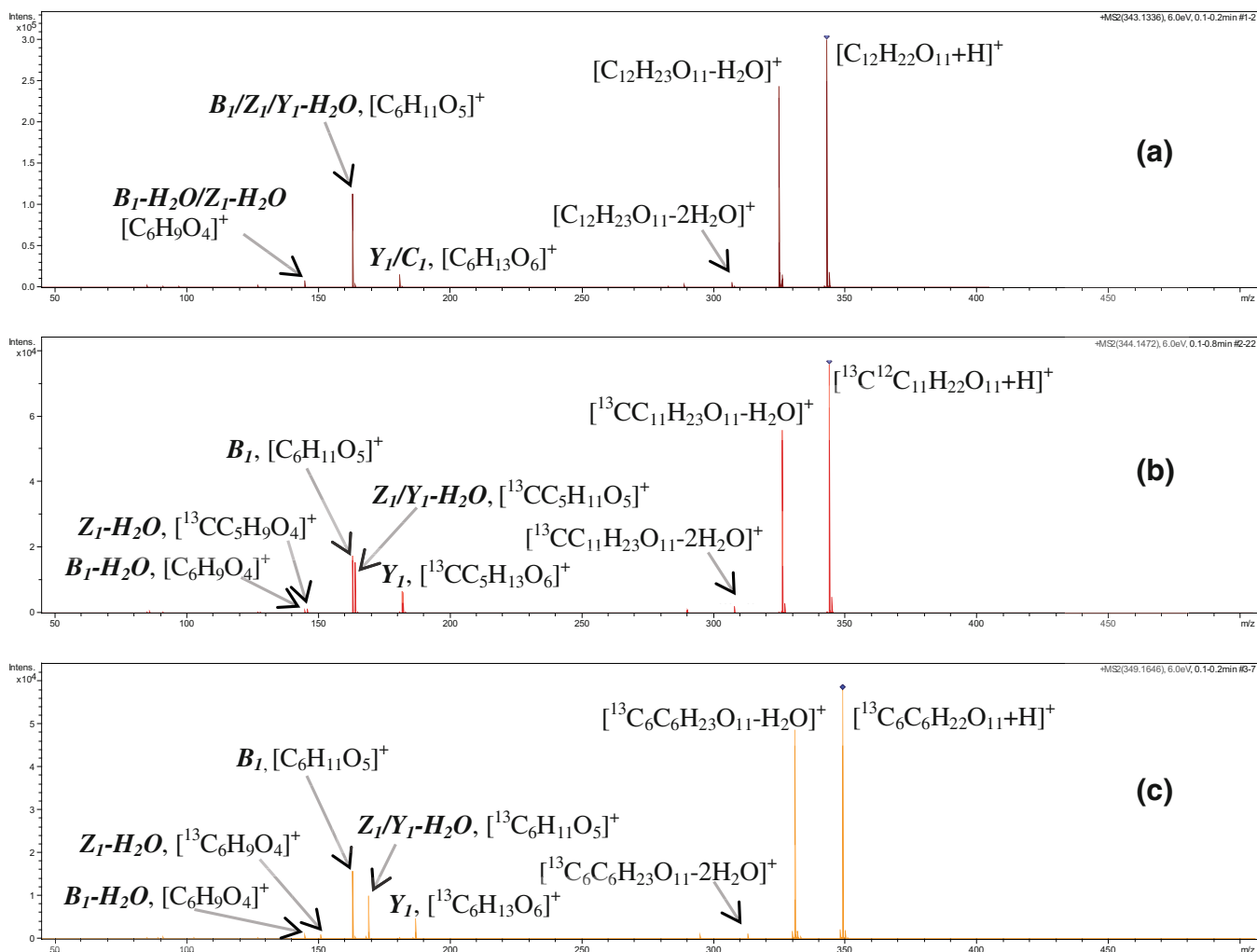


**Figure 2.** Selected protonated lactose MS/MS spectra: **(a)** unlabeled protonated lactose  $[\text{C}_{12}\text{H}_{22}\text{O}_{11} + \text{H}]^+$ ; **(b)** singly, regioselectively  $^{13}\text{C}$ -labeled lactose ( $^{13}\text{C}_1$ -labeled glucose carbon 1)  $[^{13}\text{C}^{12}\text{C}_{11}\text{H}_{22}\text{O}_{11} + \text{H}]^+$ ; **(c)** regioselectively  $^{13}\text{C}$ -labeled lactose ( $^{13}\text{C}_6$ -labeled glucose carbons 1-6);  $[^{13}\text{C}_6^{12}\text{C}_6\text{H}_{22}\text{O}_{11} + \text{H}]^+$

coordination by a greater number of oxygen atoms to the larger cations limiting the ability for glycosidic and other bond cleavages to occur at low collision energies when larger metal ions are present. In the following sections, we will discuss the structural and mechanistic consequences of varying the choice of cation with the aid of our computations and tandem mass spectra.

### Cationization Energetics

Our calculations indicate that the bonding arrangements vary considerably between the protonated and metal-cationized forms of lactose. The heavier metal cations have greater ionic radii and thus can accommodate more oxygen atoms to solvate the positive charge (typically up to 4 oxygens coordinating rather than 2). For example, in the most energetically favorable cationized conformer of  $\beta$ -D-galactopyranosyl-(1 $\rightarrow$ 4)- $\beta$ -D-glucose, the primary cation–oxygen bond distances are:  $\text{H}^+$ , 1.09–1.36 Å <  $\text{Li}^+$ , 1.89–2.10 Å <  $\text{Na}^+$ , 2.22–2.38 Å <  $\text{K}^+$ , 2.60–2.82 Å. The lowest energy conformer is very similar even as the cation is varied (Supplementary Figure S1). This leads to

slightly larger ion structures, consistent with recent ion-mobility data [28, 46].

For the protonated systems, there are a large number of low energy conformers owing to the multitude of energetically similar hydroxyl protonation sites (Tables 1 and 2). Both anomeric forms of protonated lactose have protonation of the hydroxyl oxygen attached to carbon 6 of the galactose ( $C6\_Gal$ ) as the minimum energy structure. The most energetically favorable metal-cationized forms have a higher degree of coordination than their protonated congeners, leading to fewer distinct structures (Tables 3 and 4). Nevertheless, there are a significant number of structures that can potentially be populated following collisional activation.

### Glycosidic Bond Cleavage Transition Structures: the $B_n$ - $Y_m$ Pathways

Our calculations predict substantial energetic differences between the protonated and sodiated lactose analytes. In

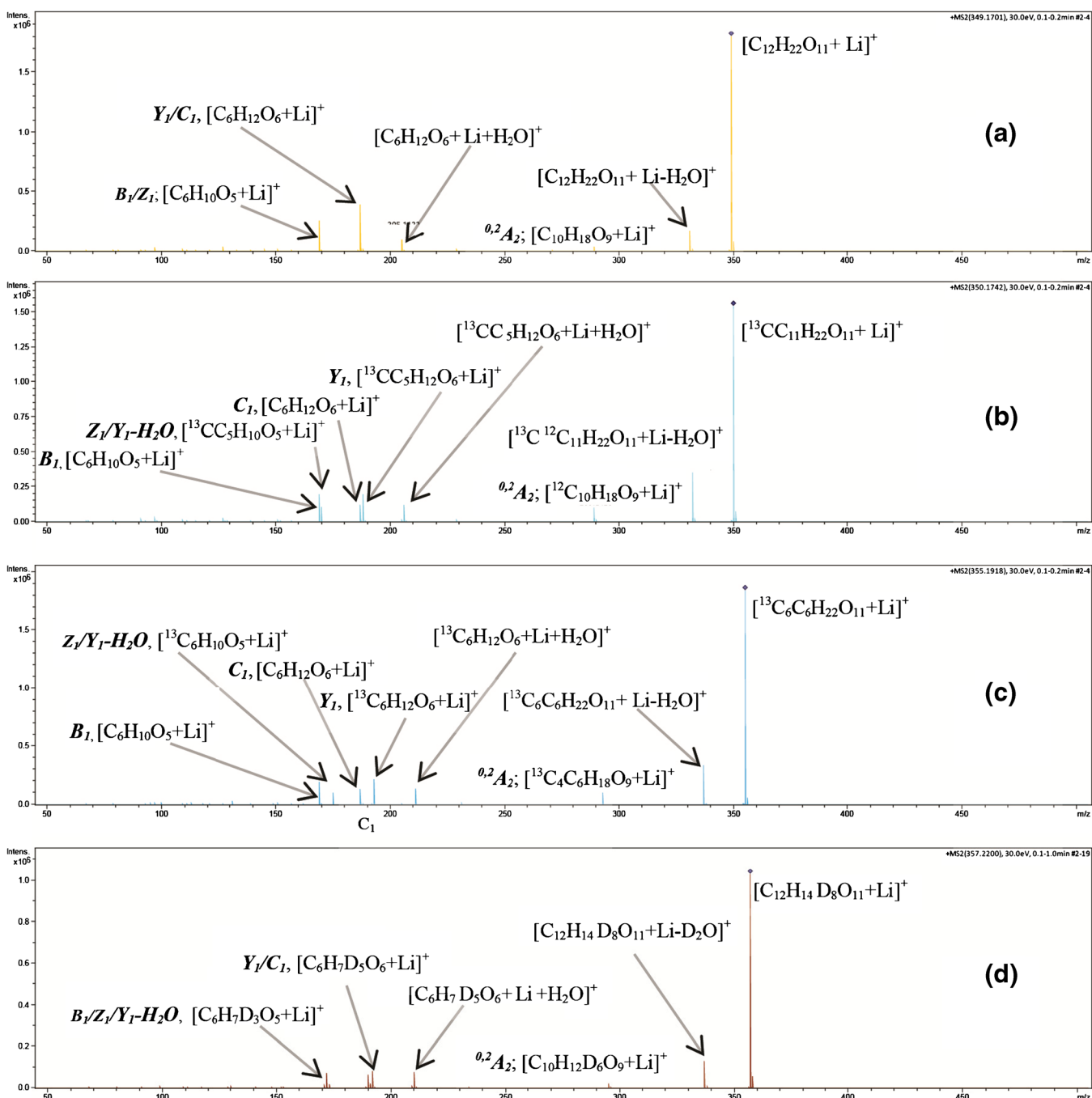


**Figure 3.** Selected lithiated lactose MS/MS spectra: **(a)** unlabeled lithiated lactose  $[C_{12}H_{22}O_{11} + Li]^+$ ; **(b)** singly, regioselectively  $^{13}C$ -labeled lithiated lactose ( $^{13}C_1$ -labeled glucose carbon 1)  $[^{13}C^{12}C_{11}H_{22}O_{11} + Li]^+$ ; **(c)** lithiated regioselectively  $^{13}C$ -labeled lactose ( $^{13}C_6$ -labeled glucose carbons 1-6)  $[^{13}C_6^{12}C_6H_{22}O_{11} + Li]^+$ ; **(d)** lithiated lactose with all eight hydroxyl protons exchanged for deuterons  $[C_{12}H_{14}D_8O_{11} + Li]^+$

agreement with experiment, the heavier cation requires additional energy to cleave the glycosidic bond. For example, the glycosidic bond cleavage  $B_I$ - $Y_I$  transition structures for the protonated congeners require only 143.1 and 138.3  $\text{kJ mol}^{-1}$  to access for the  $\alpha$  and  $\beta$  anomers ( $\Delta E_{\text{cl}+ZPE,0\text{K}}$ , Tables 1 and 2). In contrast, the glycosidic bond cleavage  $B_I$ - $Y_I$  transition structures of the sodiated forms require at least 248.3 and

245.6  $\text{kJ mol}^{-1}$  ( $\Delta E_{\text{cl}+ZPE,0\text{K}}$ , Tables 3 and 4). How do these reactions proceed?

For the protonated forms, our calculations predict two energetically very similar processes to be responsible for glycosidic bond cleavage. The  $\beta$ -D-galactopyranosyl-(1 $\rightarrow$ 4)- $\alpha$ -D-glucose form marginally favors concerted cyclization and glycosidic bond cleavage to form a

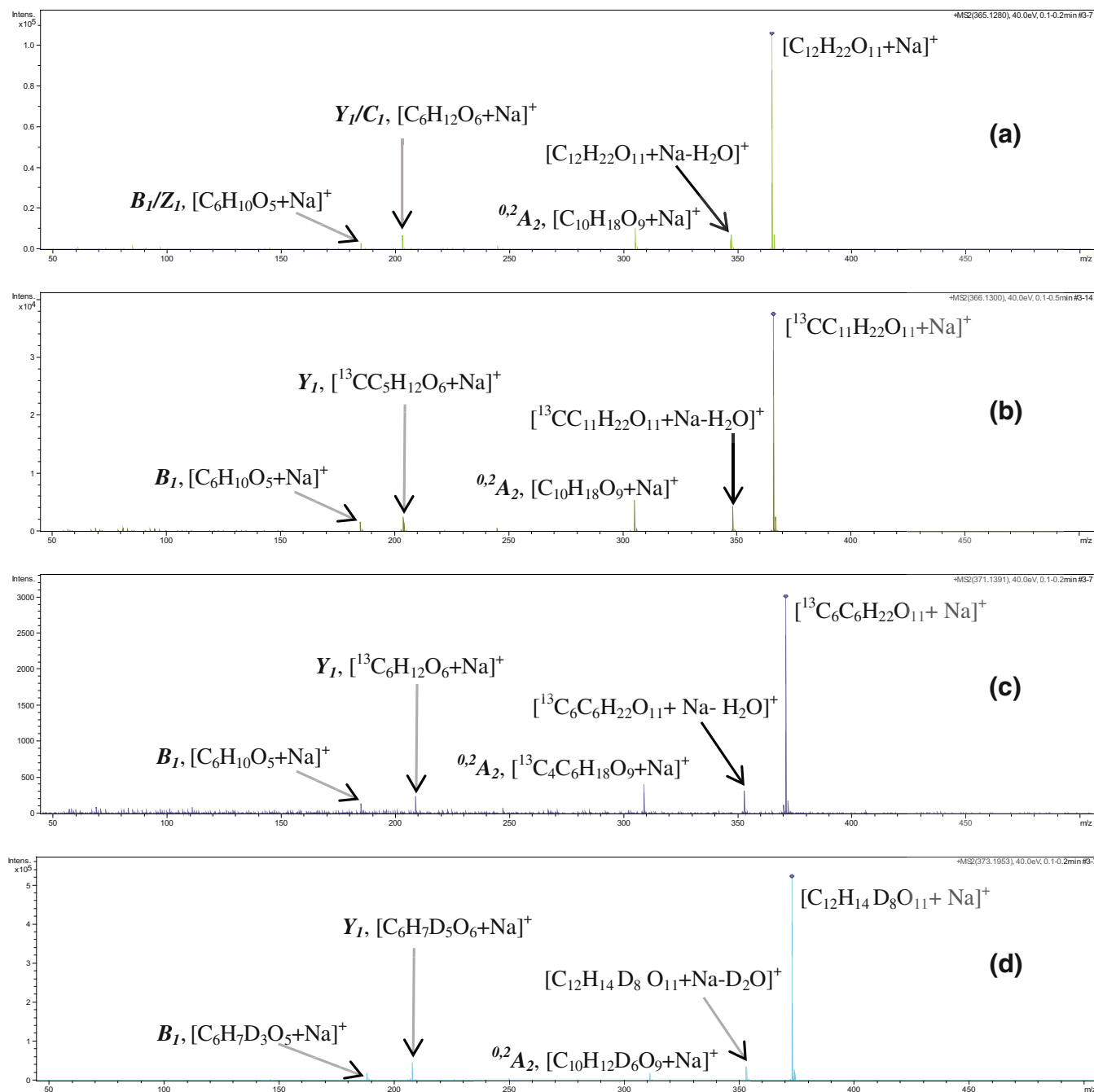


**Figure 4.** Selected sodiated lactose MS/MS spectra: **(a)** unlabeled sodiated lactose  $[C_{12}H_{22}O_{11}+Na]^+$ ; **(b)** singly, regioselectively  $^{13}C$ -labeled sodiated lactose ( $^{13}C_1$ -labeled glucose carbon 1)  $[^{13}C_1,^{12}C_{11}H_{22}O_{11}+Na]^+$ ; **(c)** regioselectively  $^{13}C$ -labeled sodiated lactose ( $^{13}C_6$ -labeled glucose carbons 1-6)  $[^{13}C_6,^{12}C_6H_{22}O_{11}+Na]^+$ ; **(d)** sodiated lactose with all eight hydroxyl protons exchanged for deuterons  $[C_{12}H_{14}D_8O_{11}+Na]^+$

protonated 1,6-anhydrogalactose ion (Scheme 1a, Supplementary Figure S2a), whereas the lowest energy glycosidic bond cleavage of  $\beta$ -D-galactopyranosyl-(1 $\rightarrow$ 4)- $\beta$ -D-glucose forms an oxacarbenium ion (Scheme 1b, Supplementary Figure S2b). Although the initially generated proton-bound dimer product structures differ (Scheme 1), both pathways are initiated by mobilization [47–54] of a proton to the glycosidic bond. The reactive configurations (Supplementary Figure S2) are formed by rotation of the

reducing (glucose) end of the ion with the ionizing proton located on the galactose carbon 6 hydroxyl oxygen being solvated by the glycosidic oxygen. The difference between the two reactive configuration types is in the degree of the glucose residue rotation. This rotation affects the more peripheral hydrogen-bonding and, critically, the position of the galactose carbon 6 hydroxyl group (Supplementary Figure S2). In both cases, proton transfer and glycosidic bond cleavage occur in a concerted manner (Scheme 1,

**Table 1.** Relative Energies of the Minima and Transition Structures of [ $\beta$ -D-Galactopyranosyl-(1 $\rightarrow$ 4)- $\alpha$ -D-Glucose + H]<sup>+</sup> Ion Calculated at the M06-2X/6-31+G(d,p) Level of Theory

	$E_{cl}/H$	$E_{cl+ZPE}/H$	$\Delta E_{cl+ZPE,0K}/\text{kJ mol}^{-1}$	$\Delta H_{298}/\text{kJ mol}^{-1}$	$\Delta G_{298}/\text{kJ mol}^{-1}$	$\Delta S_{298}/\text{J mol}^{-1}$
C1_Gal (Glycosidic bond)	-1297.867345	-1297.476182	115.2	118.2	109.2	34.9
C2_Gal	-1297.89556	-1297.504288	41.4	41.1	41.5	-1.7
C3_Gal	-1297.884037	-1297.491582	78.4	75.3	72.5	10.9
C4_Gal	-1297.879681	-1297.491481	75.0	79.5	67.6	46.2
C5_Gal	-1297.865184	-1297.484772	92.6	96.0	85.4	41.4
C6_Gal	-1297.911315	-1297.520057	0	0	0	0
C1_Glu	-1297.872652	-1297.483550	95.8	98.1	92.6	21.4
C2_Glu	-1297.870875	-1297.478559	109.0	110.0	106.4	13.7
C3_Glu	-1297.878087	-1297.488471	82.9	86.2	76.0	39.7
C5_Glu	-1297.852887	-1297.461424	153.9	156.3	147.4	34.6
C6_Glu	-1297.893882	-1297.503422	43.7	44.4	41.5	11.1
1,6-Anhydrogalactose ion cyclization	-1297.854695	-1297.465541	143.1	146.5	134.5	46.7
B <sub>1</sub> -Y <sub>1</sub> TS Cleavage						
Oxacarbenium ion B <sub>1</sub> -Y <sub>1</sub> TS	-1297.851247	-1297.464306	146.4	152.0	138.3	53.4
Proton-bound dimer cyclization B <sub>1</sub> -Y <sub>1</sub> TS	-1297.853854	-1297.465037	144.5	148.3	136.6	45.3
C <sub>1</sub> -Z <sub>1</sub> TS glycosidic bond Cleavage	-1297.823771	-1297.436231	220.1	224.6	210.6	54.3
H <sub>2</sub> O-loss TS C <sub>1</sub> _Glu	-1297.852400	-1297.465439	143.4	148.7	134.6	54.7
H <sub>2</sub> O-loss TS C <sub>2</sub> _Gal	-1297.829890	-1297.440099	207.6	211.0	201.4	37.1
B <sub>1</sub> <sup>-H<sub>2</sub>O</sup> -Y <sub>1</sub> TS Glycosidic bond Cleavage	-1297.807171	-1297.425588	248.0	258.2	193.1	252.8
B <sub>1</sub> -Y <sub>1</sub> <sup>-H<sub>2</sub>O</sup> TS Glycosidic bond Cleavage	-1297.810540	-1297.428871	239.4	248.4	188.6	232.2

Glu = glucose; Gal = galactose

Supplementary Figure S3) to produce a proton-bound dimer of a B<sub>1</sub> ion and glucose. Direct separation of this dimer in each case results in detection of a B<sub>1</sub> ion, whereas rearrangement of, and proton transfer from, the B<sub>1</sub> ion prior to complex dissociation results in Y<sub>1</sub> ion (protonated glucose) formation. Our calculations indicate that 1,2-anhydrogalactose, the neutral form of the oxacarbenium B<sub>1</sub> ion (Scheme 1b), has a proton affinity of ~858 kJ mol<sup>-1</sup>, which is larger than that of glucose ( $\alpha$  ~850,  $\beta$  ~843 kJ mol<sup>-1</sup>, see also [55]). So from this pathway, you would expect to produce B<sub>1</sub> ions [56] rather than protonated  $\beta$ -glucose, which is broadly consistent with the

relative peak intensities of <sup>13</sup>C-labeled experimental data (Figure 2). Additionally, the  $\beta$ -D-galactopyranosyl-(1 $\rightarrow$ 4)- $\beta$ -D-glucose anomer is typically more abundant (~60:40 [57]) than the  $\alpha$ -anomer, so this likely explains some of the B<sub>1</sub> ion current. In contrast, the 1,6-anhydrogalactose isomer only has a proton affinity of ~813 kJ mol<sup>-1</sup>, which is substantially lower than that of  $\alpha$ -glucose, thus primarily leading to Y<sub>1</sub> ion production [56]. Interconversion of these isomers within the proton-bound dimer is also energetically possible (144.5 and 144.9 kJ mol<sup>-1</sup>, Supplementary Scheme S1), although this process is of debatable thermodynamic benefit as the two potential B<sub>1</sub> ion structures are equi-energetic with ~1.7 kJ mol<sup>-1</sup> between them. To complicate

**Table 2.** Relative Energies of the Minima and Transition Structures of [ $\beta$ -D-Galactopyranosyl-(1 $\rightarrow$ 4)- $\beta$ -D-Glucose + H]<sup>+</sup> Ion Calculated at the M06-2X/6-31+G(d,p) Level of Theory

	$E_{cl}/H$	$E_{cl+ZPE}/H$	$\Delta E_{cl+ZPE,0K}/\text{kJ mol}^{-1}$	$\Delta H_{298}/\text{kJ mol}^{-1}$	$\Delta G_{298}/\text{kJ mol}^{-1}$	$\Delta S_{298}/\text{J mol}^{-1}$
C1_Gal (Glycosidic bond)	-1297.851641	-1297.460792	150.0	153.4	144.1	36.1
C2_Gal	-1297.892150	-1297.501454	43.2	43.2	42.2	3.7
C3_Gal	-1297.881261	-1297.489204	75.4	76.0	72.8	12.6
C4_Gal	-1297.880021	-1297.491783	68.6	72.9	60.9	46.5
C5_Gal	-1297.874814	-1297.484288	88.3	91.8	80.2	44.8
C6_Gal	-1297.909011	-1297.517911	0	0	0	0
C1_Glu	-1297.861578	-1297.471403	122.1	123.9	115.9	31.3
C2_Glu	-1297.85942	-1297.468883	128.7	131.2	124.7	25.2
C3_Glu	-1297.881045	-1297.491926	68.2	71.0	62.1	34.6
C5_Glu	-1297.859741	-1297.859741	126.0	130.4	117.3	50.8
C6_Glu	-1297.879431	-1297.491435	69.5	72.4	63.1	36.2
1,6-Anhydrogalactose ion cyclization	-1297.851863	-1297.463471	142.9	146.8	133.1	53.4
B <sub>1</sub> -Y <sub>1</sub> TS Cleavage						
Oxacarbenium ion B <sub>1</sub> -Y <sub>1</sub> TS	-1297.853031	-1297.465253	138.3	143.4	130.8	48.7
Proton-bound dimer cyclization B <sub>1</sub> -Y <sub>1</sub> TS	-1297.850840	-1297.462727	144.9	149.3	135.7	52.9
C <sub>1</sub> -Z <sub>1</sub> TS glycosidic bond Cleavage	-1297.816793	-1297.429495	232.1	237.1	221.8	29.1
H <sub>2</sub> O-loss TS C <sub>1</sub> _Glu	-1297.839226	-1297.453751	168.5	175.7	155.4	78.8
H <sub>2</sub> O-loss TS C <sub>2</sub> _Gal	-1297.826351	-1297.438687	208.0	212.6	199.0	52.6
B <sub>1</sub> <sup>-H<sub>2</sub>O</sup> -Y <sub>1</sub> TS glycosidic bond Cleavage	-1297.807171	-1297.425588	242.4	252.7	187.0	254.7
B <sub>1</sub> -Y <sub>1</sub> <sup>-H<sub>2</sub>O</sup> TS glycosidic bond Cleavage	-1297.810540	-1297.428871	233.8	242.9	182.5	234.2

Glu = glucose; Gal = galactose

**Table 3.** Relative Energies of the Minima and Transition Structures of [ $\beta$ -D-Galactopyranosyl-(1 $\rightarrow$ 4)- $\alpha$ -D-glucose + Na] $^+$  Ion Calculated at the M06-2X/6-31+G(d,p) Level of Theory

	$E_{cl}/H$	$E_{cl+ZPE}/H$	$\Delta E_{cl+ZPE,0K}/kJ\ mol^{-1}$	$\Delta H_{298}/kJ\ mol^{-1}$	$\Delta G_{298}/kJ\ mol^{-1}$	$\Delta S_{298}/J\ mol^{-1}$
(C2,Gal)Na(C1,Gal)	-1459.669247	-1459.288324	50.0	50.4	48.4	6.5
(C2,Gal)Na(C3,Gal)	-1459.669454	-1459.287859	51.2	50.9	50.6	0.9
(C3,Gal)Na(C4,Gal)	-1459.676518	-1459.294385	34.1	32.8	34.5	-5.7
(C4,Gal)Na(C6,Gal)	-1459.668250	-1459.286650	50.2	50.3	49.2	3.7
(C4,C6,C5,Gal)Na(C6,Glu)	-1459.688904	-1459.304081	0	0	0	0
(C1, Glu)Na(C5,Glu)	-1459.64466	-1459.263778	114.4	115.0	111.6	11.4
(C1, Glu)Na(C2,Glu)	-1459.647608	-1459.267301	105.2	106.9	99.3	25.4
(C2, Glu)Na(C3,Glu)	-1459.669462	-1459.287982	50.9	50.6	49.3	4.2
B <sub>1</sub> -Y <sub>1</sub> TS glycosidic bond cleavage	-1459.590511	-1459.212788	248.3	249.6	241.6	26.6
B <sub>1</sub> -Y <sub>1</sub> TS (C <sub>alpha</sub> -H) glycosidic bond cleavage	-1459.583738	-1459.210273	249.2	251.7	245.6	20.6
Proton-bound dimer cyclization B <sub>1</sub> -Y <sub>1</sub> TS	-1459.587175	-1459.209940	255.8	257.0	250.1	23.0
C <sub>1</sub> -Z <sub>1</sub> TS glycosidic bond cleavage	-1459.561620	-1459.186325	317.8	320.6	310.0	35.5
Glucose ring-opening TS	-1459.598670	-1459.223883	219.2	219.6	217.1	8.4
<sup>0,2</sup> A <sub>2</sub> TS cross-ring cleavage	-1459.596612	-1459.224317	218.0	220.3	215.7	15.7
<sup>2,4</sup> A <sub>2</sub> TS cross-ring Cleavage	-1459.545931	-1459.176811	342.8	348.0	282.5	219.6

Glu = glucose; Gal = galactose

matters further, generation of B<sub>1</sub> ion current from consecutive reactions is also potentially possible.

Furthermore, the threshold relative energy of the separated B<sub>1</sub> ion and neutral glucose products is substantially higher ( $\Delta E_{cl+ZPE,0K} = 234.1$  and  $230.4\ kJ\ mol^{-1}$ ) than both the glycosidic bond cleavage transition structure and the potential B<sub>1</sub> ion isomerization barrier. This indicates the stabilization provided by hydrogen bonding between the fragments in the proton-bound dimer is much larger than the sum of that available to either fragment when alone. This finding is supported by blackbody infrared radiative dissociation (BIRD) data from the Klassen group [22]. Their experiments on larger protonated glycans provided small pre-exponential factors when generating B<sub>n</sub> ions which are not consistent with simple bond fission as the rate-determining step. How much of the various processes occur will be a function of how long the dimers remain in physical contact; as collision energies increase and thus the internal energy of each analyte increases, the lifetime of the dimers should reduce, thereby making interconversion less likely. Our experiments

are clearly at energies substantially above the threshold for fragmentation, so in principle should favor comparatively prompt dimer separation and consecutive reactions too (supported by MS<sup>3</sup> data and the recent literature [22]). The combined chemistries (and thus, rates) make simple, proton affinity-based predications of the overall B<sub>n</sub>/Y<sub>m</sub> ion branching ratio far less reliable, unlike for simple aliphatic peptide systems [58].

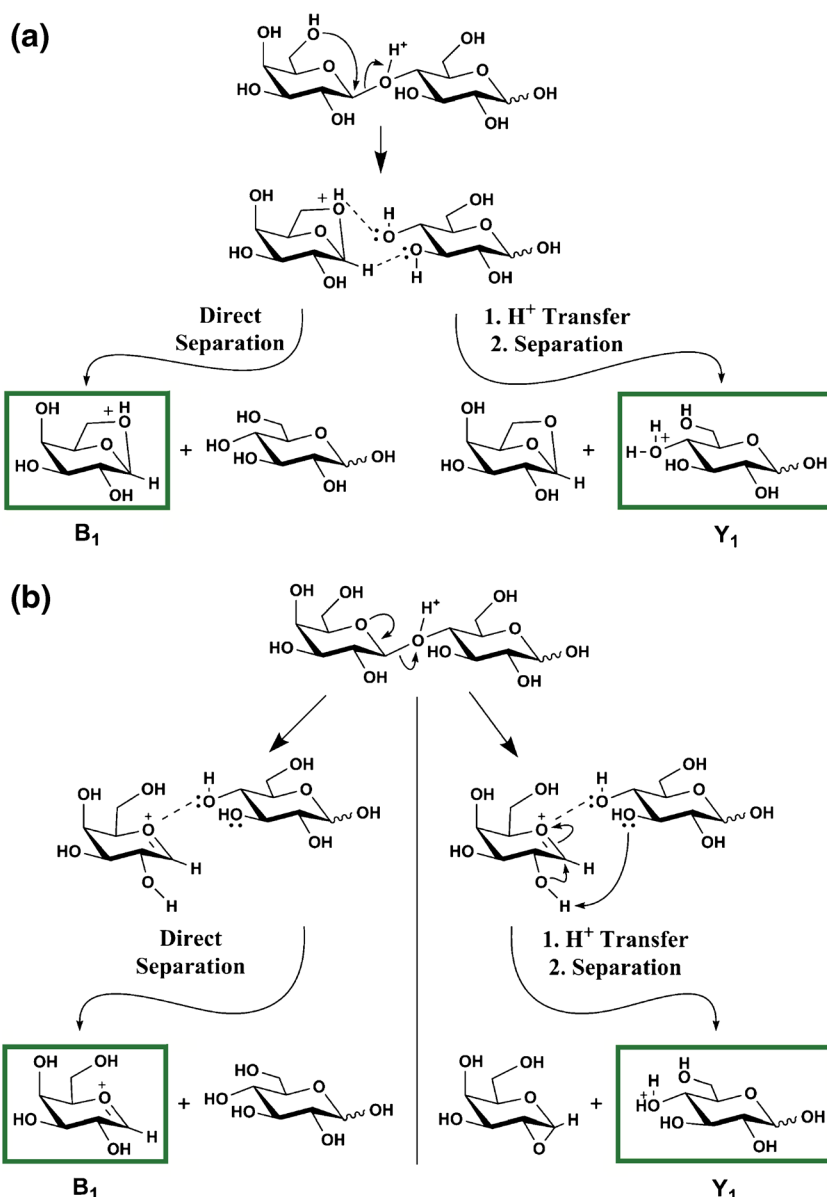
Glycosidic bond cleavage in the sodiated system offers more possibilities because of differences in glycosidic bond cleavage initiated by proton and sodium cation. Consequently, there are numerous B<sub>1</sub>-Y<sub>1</sub> transition structures to consider in addition to the direct congeners of the protonated system. Our deuterium labeling data indicates that the B<sub>1</sub> ion detected has three D atoms and the complementary Y<sub>1</sub> ion has five D atoms. This is consistent with the earlier deuterated [gentiobiose + Li] $^+$  data [17]. Thus, one of the deuterons from the non-reducing,  $\beta$ -D-galactose end of the molecule needs to be transferred to the glucose end, either prior to glycosidic bond cleavage, or in the proton-bound dimer before dissociation. Why might this be a problem?

**Table 4.** Relative Energies of the Minima and Transition Structures of [ $\beta$ -D-Galactopyranosyl-(1 $\rightarrow$ 4)- $\beta$ -D-Glucose + Na] $^+$  Ion Calculated at the M06-2X/6-31+G(d,p) Level of Theory

	$E_{cl}/H$	$E_{cl+ZPE}/H$	$\Delta E_{cl+ZPE,0K}/kJ\ mol^{-1}$	$\Delta H_{298}/kJ\ mol^{-1}$	$\Delta G_{298}/kJ\ mol^{-1}$	$\Delta S_{298}/J\ mol^{-1}$
(C2,Gal)Na(C1,Gal)	-1459.669031	-1459.288118	41.9	43.8	38.2	18.6
(C2,Gal)Na(C3,Gal)	-1459.671158	-1459.290067	36.8	38.3	32.7	19.0
(C3,Gal)Na(C4,Gal)	-1459.673796	-1459.292239	31.1	32.1	27.4	15.9
(C4,Gal)Na(C6,Gal)	-1459.671119	-1459.289857	37.3	39.1	33.4	19.0
(C4,C6,C5,Gal)Na(C6,Glu)	-1459.684952	-1459.304081	0	0	0	0
(C1,Glu)Na(C5,Glu)	-1459.668799	-1459.288018	42.2	44.5	38.7	19.4
(C1Glu)Na(C2,Glu)	-1459.646906	-1459.266775	97.9	100.9	90.3	35.6
(C2,Glu)Na(C3,Glu)	-1459.667016	-1459.285516	48.7	50.0	44.9	17.0
B <sub>1</sub> -Y <sub>1</sub> TS glycosidic bond cleavage	-1459.587853	-1459.210526	245.6	248.7	237.0	39.1
B <sub>1</sub> -Y <sub>1</sub> TS (C <sub>alpha</sub> -H) Glycosidic bond cleavage	-1459.583738	-1459.210273	246.3	251.1	238.6	41.9
Proton-bound dimer cyclization B <sub>1</sub> -Y <sub>1</sub> TS	-1459.584386	-1459.207618	253.3	256.4	244.4	40.1
C <sub>1</sub> -Z <sub>1</sub> TS Glycosidic bond cleavage	-1459.554405	-1459.179572	326.9	331.8	316.1	52.6
Glucose ring-opening TS	-1459.601692	-1459.226046	204.9	206.6	204.0	8.8
<sup>0,2</sup> A <sub>2</sub> TS Cross-ring cleavage	-1459.596612	-1459.224317	209.4	213.3	204.5	29.6
<sup>2,4</sup> A <sub>2</sub> TS Cross-ring cleavage	-1459.545931	-1459.176811	334.1	341.0	271.3	233.5

Glu = glucose; Gal = galactose



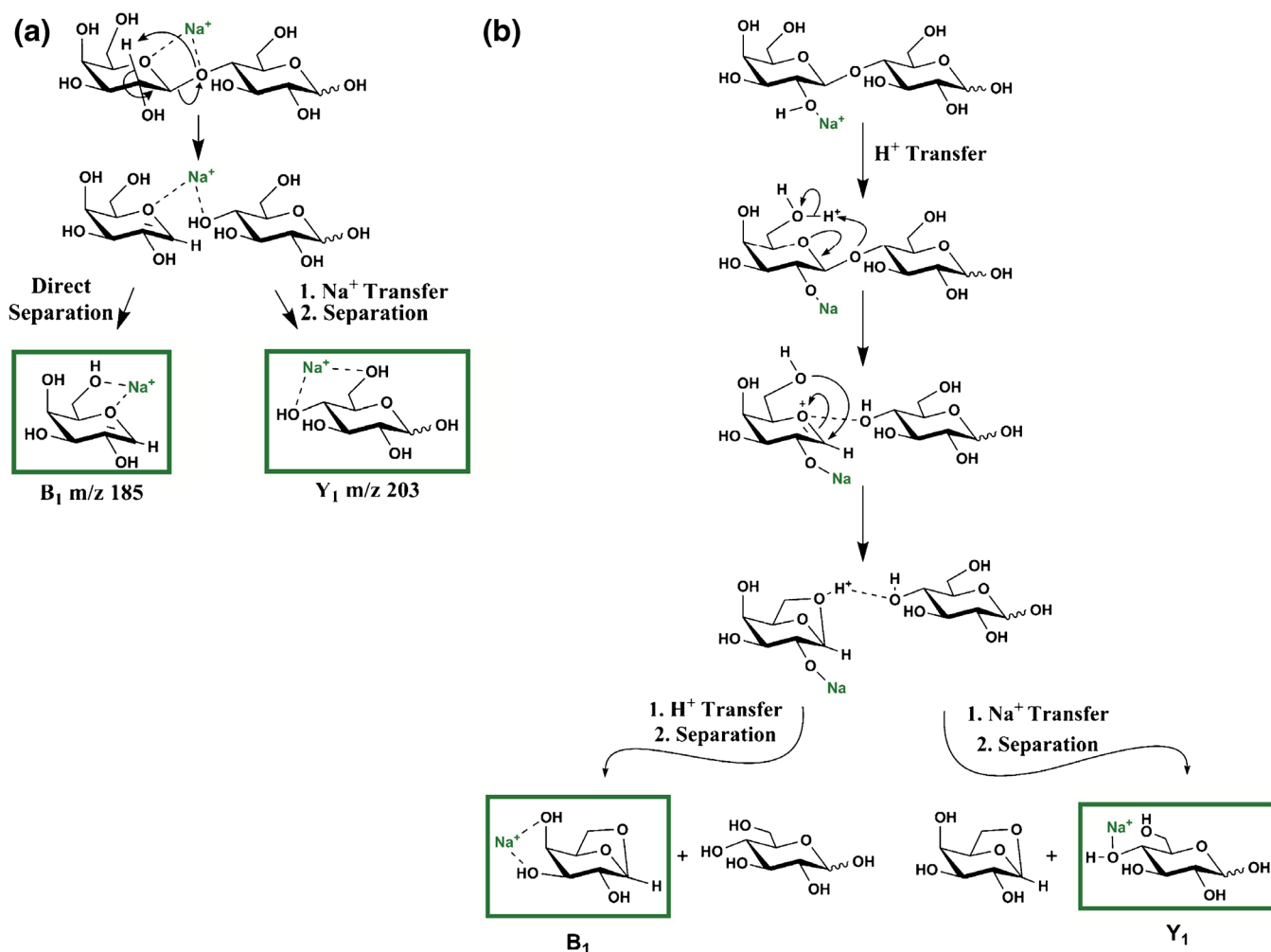


**Scheme 1.** Simplified  $B_1$ - $Y_1$  fragmentation pathways for protonated lactose, [lactose +  $H$ ] $^+$ . (a) The direct, 1,6-anhydrogalactose ion-forming  $B_1$ - $Y_1$  pathway and (b) The oxocarbenium ion-forming  $B_1$ - $Y_1$  pathway

Traditionally, it has been argued that direct coordination of the metal to the glycosidic oxygen was a prerequisite for bond cleavage (just like in Scheme 1b). In the present case, when we optimized transition structures in this manner (i.e., analogous to the protonated case), we instead observe a different chemistry. The glycosidic oxygen abstracts the galactose  $C_{2\alpha}$  proton instead to produce a 2-hydroxygalactal structure as the non-reducing fragment. This requires 249.2 or 246.3  $\text{kJ mol}^{-1}$  for the  $\alpha$  and  $\beta$  anomers ( $\Delta E_{\text{el+ZPE,0K}}$ ,  $C_{\alpha\text{H}}$  abstraction  $B_1$ - $Y_1$  TS, Tables 3 and 4, Scheme 2a, Supplementary Scheme S2a, Figure 5a) at the M06-2X/6-31+G(d,p) level of theory. Subsequently, an ion-molecule dimer is generated in which the sodiated 2-hydroxygalactal  $B_1$  ion retains 4 deuterons. Direct separation of this dimer would produce a  $B_1$  ion peak at  $m/z$  189, rather than the experimental  $m/z$  188. Using the same logic, the

$Y_1$  ion would appear 1 u lower than the experiment ( $m/z$  208), at  $m/z$  207 (Supplementary Scheme S2). Unless the abstracted  $C_{2\alpha}$  proton is exchanged for a deuteron from the galactyl  $B_1$  ion in the proton-bound dimer in essentially every case, this mechanism cannot predominate.

The major alternatives to this mechanism are ones in which the sodium is located between either two alcohol groups of a single residue or bridged between alcohol groups from both residues, but not the glycosidic oxygen. A proton (deuteron) is then mobilized to the glycosidic bond to facilitate cleavage. We have examined many of these possibilities, and only one is competitive with the  $C_{\alpha\text{H}}$  abstraction  $B_1$ - $Y_1$  mechanism described above, at this level of theory. We find no evidence for the previous proposal [17], in which it was argued that the non-reducing residue C2 alcohol group must provide the



**Scheme 2.** The energetically competitive  $B_1$ - $Y_1$  fragmentation pathways for sodiated lactose,  $[\text{lactose} + \text{Na}]^+$ . **(a)**  $B_1$ - $Y_1$  TS ( $C_{\alpha\text{H}}$ -H) and **(b)**  $B_1$ - $Y_1$  TS

proton (deuteron) for abstraction by the glycosidic oxygen for incorporation into the reducing end fragment. In contrast, our calculations indicate that the proton is supplied by the C6 alcohol group (Scheme 2b, Figure 5b) following shuttling of protons around the galactyl alcohol groups. So based on the calculations, the previous proposal [17] was correct in the need for glycosidic bond protonation, just not in the exact means by which this could be achieved most readily. In fact, the glycosidic bond cleavage TSs for this mechanism are marginally more favorable at 248.3 and 245.6  $\text{kJ mol}^{-1}$  ( $B_1$ - $Y_1$  TS, Tables 3 and 4) than the  $C_{\alpha\text{H}}$ -H abstraction  $B_1$ - $Y_1$  TS glycosidic bond cleavage mechanism (249.2 or 246.3  $\text{kJ mol}^{-1}$ ). However, this ‘difference’ is tiny, and certainly within the expected uncertainty of the calculation method. This prompted us to investigate whether this computational result was affected either by a larger basis set or different model chemistry. Targeted single point calculations using the M06-2X and MP2 levels of theory with the much larger 6-311++G(2d,p) basis set were performed on select precursor and transition structures to assess variability in the description of the chemistry (summarized in Table 5). The M06-2X/6-311++G(2d,p) single point calculations do

show a shift in relative energy to favor the  $B_1$ - $Y_1$  TS, which is consistent with the labeling data. However, the relative ‘shift’ for the  $\beta$ -form is  $<1 \text{ kJ mol}^{-1}$ . More convincing are the MP2(FC)/6-311++G(2d,p) calculations, which favor  $B_1$ - $Y_1$  TS pathway over the  $C_{\alpha\text{H}}$ -H abstraction  $B_1$ - $Y_1$  TS glycosidic bond cleavage mechanism by over 32  $\text{kJ mol}^{-1}$ . Earlier density functional methods have tended to underestimate the barrier to  $C_{\alpha\text{H}}$ -H transfer(s). It remains to be seen whether the present example is symptomatic of a similar issue in M06-2X or is specific to this analyte. However, direct separation of the ion-molecule dimer generated is unfavorable as the  $B_1$  ion product requires  $>340 \text{ kJ mol}^{-1}$ . Instead, an energetically favorable next step is necessary for product generation. First, nucleophilic attack to the galactyl carbon 6 hydroxyl oxygen into carbon 1 of the oxocarbenium ion to generate a 1,6-anhydrogalactose structure occurs (Scheme 2b). This process is catalyzed by solvation of galactyl carbon 6 hydroxyl proton by the glucose residue, which lowers the TS energy to 255.8 and 253.3  $\text{kJ mol}^{-1}$  (Tables 3, 4, and 5, Figure 5c). Following either proton or sodium ion transfer within the ion-molecule dimer separation occurs to generate either the

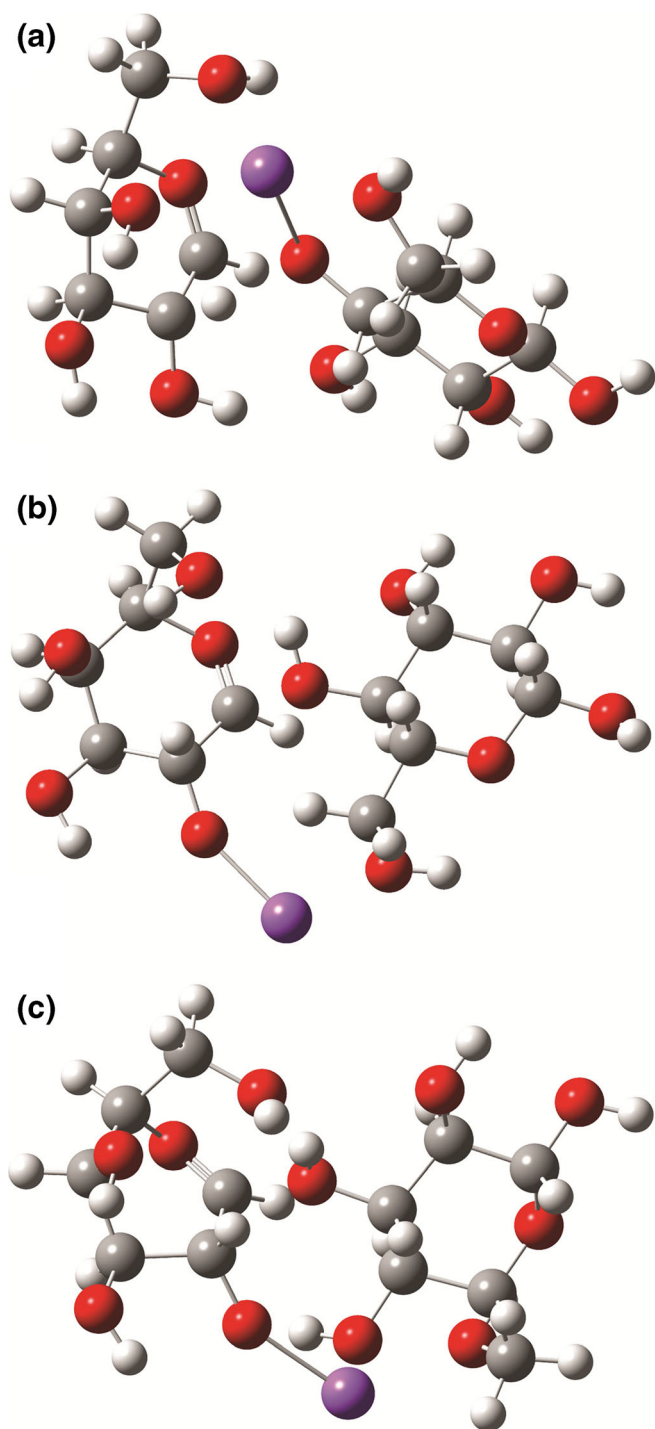


**Figure 5.** The most important transition structures of the potential  $B_1$ - $Y_1$  pathways of  $[\beta\text{-D-galactopyranosyl-(1acto}\beta\text{-D-glucose + Na)]^+$ : **(a)**  $C_{\alpha}$ -H abstraction  $B_1$ - $Y_1$  TS, **(b)**  $B_1$ - $Y_1$  TS, **(c)** glucose-catalyzed 1,6-anhydrogalactose formation in the ion-molecule dimer generated from **(b)**

sodiated 1,6-anhydrogalactose  $B_1$  ion or sodiated glucose ( $Y_1$  ion). Unlike the protonated congeners, product separation is not rate-limiting. Additionally, the competition for retention of the sodium ion is straight-forward. Our calculations indicate glucose has a sodium affinity of 183 ( $\alpha$ ) or 181 ( $\beta$ )  $\text{kJ mol}^{-1}$ ,

which are highly consistent with Heaton and Armentrout's experimental data [59]. This value is greater than 1,6-anhydrogalactose ( $173 \text{ kJ mol}^{-1}$ ), so consistent with the experimental finding of greater  $Y_1$  ion abundance than  $B_1$  ( $\sim 2:1$ , Figure 4) [56]. We are currently collecting additional data to ascertain how general this finding is.

We should note that both Suzuki et al. [37] and Yamagaki et al. [38] have previously proposed an alternate mechanism for sodiated disaccharides in which a 1,2-anhydrohexose structure is directly formed from the transition structure by way of nucleophilic attack of the galactose C2 hydroxyl oxygen into galactose C1. This proposal was based on HF/6-31G(d) calculations, which produced TSs requiring more than  $360 \text{ kJ mol}^{-1}$  for  $\beta$ -(C1) disaccharide linkage cleavages. For lactose, the non-reducing fragment neutral, 1,2-anhydrogalactose has a sodium affinity of  $230 \text{ kJ mol}^{-1}$  which would support dominant  $B_1$  ion production. We find no evidence of this mechanism being competitive here.

#### *Glycosidic Bond Cleavage Transition Structures: the $C_n$ - $Z_m$ Pathway*

Cleavage of the alternate side of the glycosidic oxygen of the protonated system also proceeds most favorably from a conformer protonated on the hydroxyl oxygen of galactose carbon 6 solvated by the glycosidic oxygen. This proton is transferred to the glycosidic oxygen, at which point the glucose ring-oxygen nucleophile attacks carbon 4 of glucose, severing the glycosidic bond while forming a new C4-O bond in a concerted manner (Scheme 3). This produces a proton-bound dimer of the newly formed  $Z_1$  ion and  $\beta$ -D-galactose residue. If this separates without any further rearrangement, a  $Z_1$  ion should be detectable. Alternatively, intracomplex proton transfer prior to dissociation results in the formation of  $C_1$  ions (protonated  $\beta$ -D-galactose in the present case). The  $C_1$ - $Z_1$  transition structure is substantially more strained than the  $B_1$ - $Y_1$  transition structure, so it is not surprising that this requires substantially more energy to access:  $220.1$  and  $232.1 \text{ kJ mol}^{-1}$  for the  $\alpha$  and  $\beta$  anomers ( $\Delta E_{\text{el}+\text{ZPE},0\text{K}}$ , Tables 1 and 2). However, the product energies are even less favorable, with the  $C_1$  ion requiring at least  $260$  and the  $Z_1 > 298 \text{ kJ mol}^{-1}$  to be formed. This is consistent with a significant portion of the ion current resulting from the compositionally identical  $Y_1^{-\text{H}_2\text{O}}$  ion. Arguments to this effect have been made previously [17, 22].

We see no evidence of the  $C_1$ - $Z_1$  pathway for sodiated lactose (Figure 4b and c). As a negative test of our approach, we performed the calculations for this system anyway. Our findings are consistent with the experimental data. The  $C_1$ - $Z_1$  glycosidic bond cleavage transition structures located for  $[\text{lactose + Na}]^+$  were much more energetically demanding;  $317.8$  and  $326.9 \text{ kJ mol}^{-1}$  for the  $\alpha$  and  $\beta$  anomers ( $\Delta E_{\text{el}+\text{ZPE},0\text{K}}$ , Tables 3 and 4). In light of this finding, the question of how demanding the subsequent dimer separation to produce sequence ions might be was not addressed specifically.

#### *Condensation Reactions and Consecutive Formation of Sequence Ions*

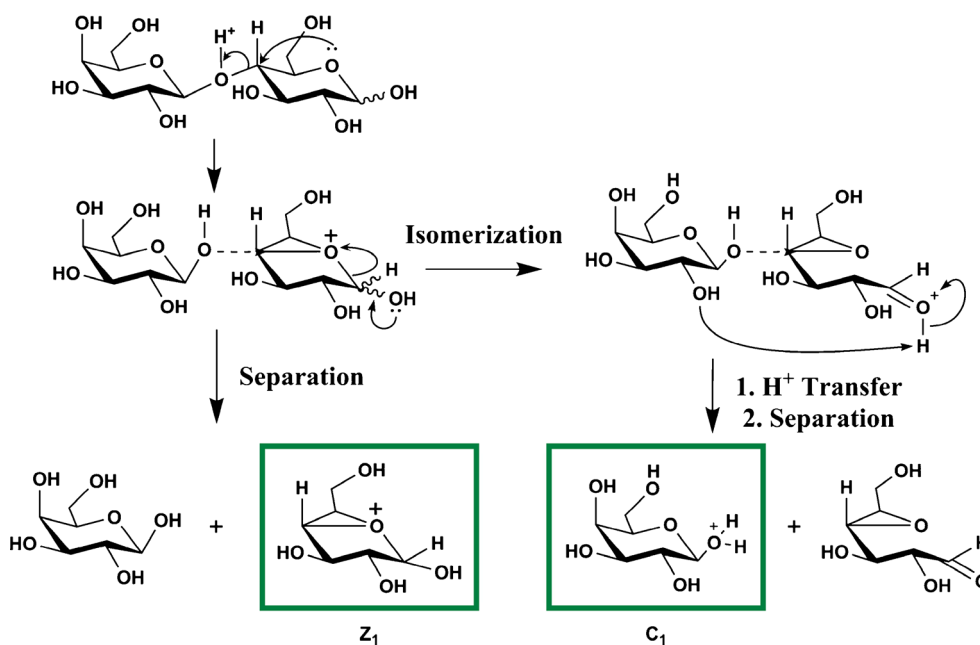
We have performed a number of investigations of water-loss pathways from the protonated congeners. This is important and

**Table 5.** Relative Energies of the  $B_1$ - $Y_1$  Transition Structures Calculated at the M06-2X/6-31+G(d,p) Level of Theory and with Single Point Energy Calculations Using the 6-31+G(d,p) Coordinates with a Larger Basis Set; M06-2X/6-311++G(2d,p)//M06-2X/6-31+G(d,p), and an Alternate Model Chemistry; MP2(FC)/6-311++G(2d,p)//M06-2X/6-31+G(d,p)

$\alpha$ -Form transition Structures	$\Delta E_{\text{cl+ZPE,0K}}/\text{kJ mol}^{-1}$		$\Delta E_{\text{cl}}/\text{kJ mol}^{-1}$	
	M06-2X/6-31+G(d,p)	M06-2X/6-311++G(2d,p)//M06-2X/6-31+G(d,p)	MP2(FC)/6-311++G(2d,p)//M06-2X/6-31+G(d,p)	$\Delta E_{\text{cl}}/\text{kJ mol}^{-1}$
$B_1$ - $Y_1$ TS Glycosidic bond cleavage	248.3		252.8	237.6
$B_1$ - $Y_1$ TS ( $C_{\alpha\text{H}}$ -H) glycosidic bond cleavage	249.2		267.4	285.7
$B_1$ - $Y_1$ TS (direct cyclization) Glycosidic bond cleavage	276.3		267.5	251.7
Proton-bound dimer cyclization $B_1$ - $Y_1$ TS	255.8		262.1	246.7
$\beta$ -Form transition structures	$\Delta E_{\text{cl+ZPE,0K}}/\text{kJ mol}^{-1}$		$\Delta E_{\text{cl}}/\text{kJ mol}^{-1}$	
	M06-2X/6-31+G(d,p)	M06-2X/6-311++G(2d,p)//M06-2X/6-31+G(d,p)	MP2(FC)/6-311++G(2d,p)//M06-2X/6-31+G(d,p)	$\Delta E_{\text{cl}}/\text{kJ mol}^{-1}$
$B_1$ - $Y_1$ TS glycosidic bond cleavage	245.6		263.8	249.5
$B_1$ - $Y_1$ TS ( $C_{\alpha\text{H}}$ -H) glycosidic bond cleavage	246.3		265.2	281.9
$B_1$ - $Y_1$ TS (direct cyclization) Glycosidic bond Cleavage	273.0		281.1	277.6
Proton-bound dimer cyclization $B_1$ - $Y_1$ TS	253.3		259.2	242.9

necessary as the [lactose +  $\text{H-H}_2\text{O}$ ] $^+$  peak is highly abundant and thus potentially encompasses the precursor ion(s) of other products. There are a large number of possible pathways depending on degree of activation [60, 61], so for brevity, our discussion is clearly not exhaustive. However, we see evidence of two primary types of pathway relevant to protonated lactose degradation and subsequent consecutive dissociations. These are (1) loss of water, which includes the anomeric oxygen, and (2) loss of water from the galactyl C2 position. The former loss has prior support in the literature from  $^{18}\text{O}$  labeling at this position [17]. The latter is a potential precursor to the  $B_1$ - $\text{H}_2\text{O}$  peaks observed in Figure 2. For loss of water from the anomeric center, our calculations support the generation of an oxacarbenium  $B_2$  ion, which is the direct congener of the  $B_1$  ion discussed previously (i.e., neither the much more strained

1,2-anhydroglucose-terminated product [17, 36] nor direct cyclization at the anomeric center (1,6-anhydroglucose-terminated product is supported). This loss proceeds through a TS at 143.4 or 168.5  $\text{kJ mol}^{-1}$  for the  $\alpha$  and  $\beta$  forms, respectively (Tables 1 and 2). At low internal (collision) energies, product separation is rate-limiting (184.3 or 190.0  $\text{kJ mol}^{-1}$ ). Alternatively, isomerization via  $\text{H}_2\text{O}$ -catalyzed cyclization of the charged-glucose end of the  $B_2$  ion in the proton bound dimer is facile (168.6 or 162.9  $\text{kJ mol}^{-1}$ , Supplementary Figure S4a) prior to separation to produce equally energetically favorable products. All of these structures are still substantially more favorable than the  $B_1$ - $Y_1$  product species, so are consistent with the experiment. Consecutive degradation of the  $B_2$  ion ( $B_1$ - $Y_1$ - $\text{H}_2\text{O}$  TS, Supplementary Figure S4b, Tables 1 and 2) requires 239.4 or 233.8  $\text{kJ mol}^{-1}$  and thus likely contributes to both the

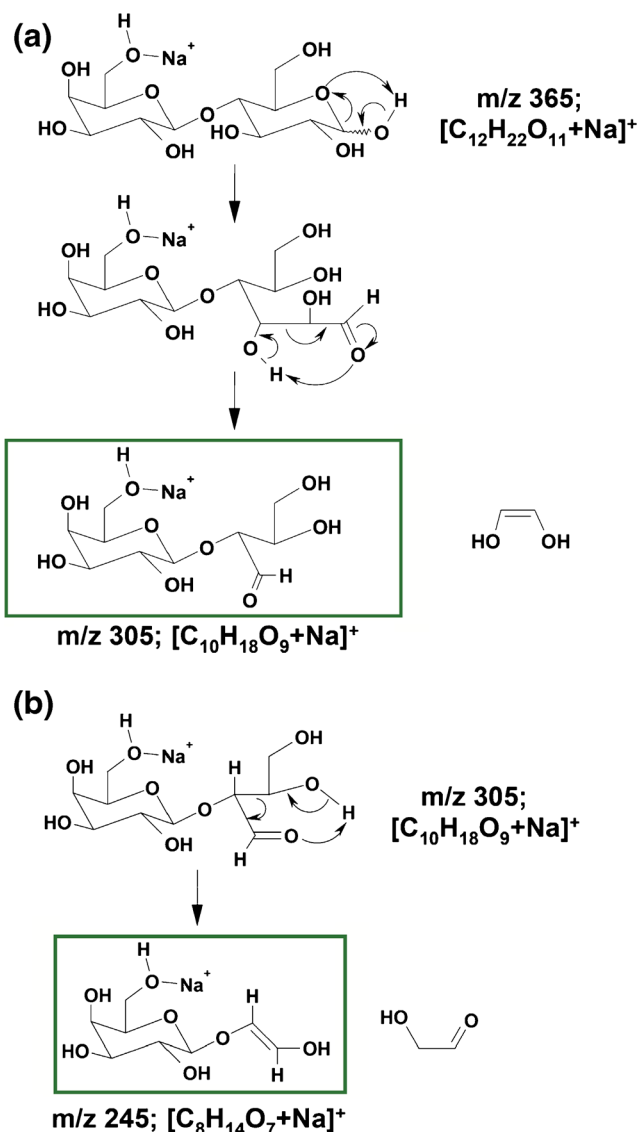
**Scheme 3.** The  $C_n$ - $Z_m$  glycosidic bond cleavage pathway for protonated lactose

$B_1$  and  $Z_1/Y_1^{-H_2O}$  peaks at increased collision energies. This is consistent with time-resolved BIRD and double-resonance experiments on carbohydrate  $B_n$  ions from the Klassen group, which provided evidence for both direct and consecutive formation of small  $B_n$  ions from larger ones. [22]

In contrast, loss of water from the galactyl C2 position is TS-limited (207.6 and 208.0 kJ mol<sup>-1</sup>). This reaction involves nucleophilic attack by the hydroxyl oxygen at C6 of the galactyl residue in an S<sub>N</sub>2-like expulsion of H<sub>2</sub>O. Recent work on protonated systems indicates that the M06-2X/6-31+G(d,p) model provides realistic estimates of S<sub>N</sub>2 reactions for protonated analytes [62], unlike some earlier density functional methods [63–66], so subsequent fragmentation of the products of this reaction as a means of producing sequence information is reasonable. Our calculations indicate that the  $B_1^{-H_2O}-Y_1$  TS generated from this ion requires at least 248.0 or 242.4 kJ mol<sup>-1</sup> to access. At higher collision energies, this will also contribute some ion current to both the  $Y_1$  and  $B_1^{-H_2O}$  peaks.

#### Cross-Ring Bond Cleavage Transition Structures: the $A_n-X_m$ Pathways

Finally we come to the cross-ring cleavage pathways that are often useful for structural elucidation. These peaks are present in the metal-cationized tandem mass spectra. For [lactose + Na]<sup>+</sup>, we observe the  $^{0,2}A_2$  peak as the most abundant sequence ion peak ( $m/z$  305, Figure 4a). Our calculations indicate the most favorable means of producing these ions is initiated by opening the D-glucose ring at the anomeric center (Scheme 4). The most favorable mechanism is charge-remote and involves local transfer of the hydroxyl proton of the anomeric center (glucose carbon 1) to the ring oxygen with concerted ring-opening. This produces an aldehyde at glucose carbon 1 and a hydroxyl group at glucose carbon 5 in direct analogy to the solution-phase reaction. This isomerization requires at least 219.2 and 204.9 kJ mol<sup>-1</sup> for the  $\alpha$  and  $\beta$  anomers ( $\Delta E_{el+ZPE,0K}$ , Tables 3 and 4, Supplementary Figure S5a). It also removes the stereocenter at the anomeric center meaning that all subsequent structures are common (note that they will have differing relative energies though, depending on whether they originated from the  $\alpha/\beta$  forms). Our regioselective <sup>13</sup>C-labeling indicates that the loss of C<sub>2</sub>H<sub>4</sub>O<sub>2</sub> comprises glucose carbons 1 and 2, rather than 5 and 6 (Figure 4b). A retro-aldol reaction has previously been proposed [17, 36] as a potential route for this decomposition (Scheme 3). Our calculations support this reaction as the most feasible pathway requiring at least 218.0 or 209.4 kJ mol<sup>-1</sup> for the  $\alpha$  and  $\beta$  anomers ( $\Delta E_{el+ZPE,0K}$ , Tables 3 and 4, Scheme 3, Supplementary Figure S5b). In addition to being the energetically most feasible sequence ion-forming pathways, and consistent with the relative peak abundances, crucially this mechanism is also consistent with our hydroxyl labeling data (Figure 4d, Supplementary Scheme S3a) (i.e., we observe a loss of 62 u corresponding to C<sub>2</sub>H<sub>2</sub>D<sub>2</sub>O<sub>2</sub>) indicating loss of an alkene-diol (HC(OD)=CH(OD), 62 u) rather than an aldehyde isomer (HC(O)-CH<sub>2</sub>(OD), 61 u).



Scheme 4. (a)  $^{0,2}A_2$  ion formation from [lactose + Na]<sup>+</sup>. (b)  $^{2,4}A_2$  ion formation from the  $^{0,2}A_2$  ion of [lactose + Na]<sup>+</sup>

At higher collision energies, the  $^{2,4}A_2$  peak is also present. Here the hydroxyl labeling data indicates a total loss of C<sub>4</sub>H<sub>5</sub>D<sub>3</sub>O<sub>4</sub>, 123 u, to give  $m/z$  250, [C<sub>8</sub>H<sub>9</sub>D<sub>5</sub>O<sub>7</sub> + Na]<sup>+</sup>. This is consistent with the consecutive fragmentation mechanism outlined in Scheme 4b and Supplementary Scheme S3b; loss of C<sub>2</sub>H<sub>2</sub>D<sub>2</sub>O<sub>2</sub> followed by loss of C<sub>2</sub>H<sub>3</sub>D<sub>1</sub>O<sub>2</sub>. Our calculations indicate that this process requires at least 342.8 or 334.1 kJ mol<sup>-1</sup> for the  $\alpha$  and  $\beta$  anomers ( $\Delta E_{el+ZPE,0K}$ , Tables 3 and 4, Supplementary Figure S5c). Although comparatively large, it is important to remember that consecutive degradation reactions are entropically very favorable due to the generation of additional gas-phase species (3 overall rather than 2 in the present case). This results in these pathways having substantially lower Gibbs free energies (282.5 and 271.3 kJ mol<sup>-1</sup>,  $\Delta G_{298K}$ , Tables 3 and 4) making them much more likely to be active at higher energies.

## Conclusions

Our combined experiments and calculations indicate that:

- (1) In agreement with the prior literature [16, 28, 35], larger group I cations require greater amounts of energy to fragment. The larger metal cations have greater ionic radii and thus can accommodate more oxygen atoms solvating the positive charge [35].
- (2) The mechanisms of the  $B_n$ - $Y_m$  fragmentation pathways of protonated and metal-cationized lactose proceed via protonation of the glycosidic oxygen with concerted glycosidic bond cleavage. In contrast with earlier proposals, our calculations predict that the sodium cation is not simultaneously coordinated to the glycosidic oxygen during this process.
- (3) Sodiation leads to transition-structure limited gas-phase fragmentation chemistry (unlike protonation). Our calculations predict that the  $B_n$  ion structures generated most readily differ markedly from those in the preceding literature. The complimentary sodium affinity thus also differs to those previously advocated, which in turn affects the product ion distribution [56]. If general this will likely lead to more accurate predictions of product ion relative abundances.
- (4) Formation of the cross-ring  $^{0,2}A_2$  and  $^{2,4}A_2$  peaks for the sodiated congeners begins with charge-remote opening of the D-glucose ring at the anomeric center. Combined  $^{13}\text{C}$  and deuterium labeling supports a retro-aldol mechanism [17, 36] for formation of the  $^{0,2}A_2$  peak with barriers that are less demanding than glycosidic bond cleavage. The less abundant  $^{2,4}A_2$  peak is a consecutive loss (of  $\text{C}_2\text{H}_3\text{D}_1\text{O}_2$ ) in an entropically favorable but energetically demanding process.
- (5) Low-energy condensation reactions ( $\text{H}_2\text{O}$ -loss) are much more prevalent for the protonated analytes. Logically, the subsequent fragmentation of the resulting product ions is also supported.
- (6) The nature of the anomeric center ( $\alpha/\beta$ ) affects the relative energies of these processes but not the overall ranking.

So where do we go from here? We intend to build on the present findings and examine a wider variety of larger, more biologically interesting systems. We shall endeavor to identify which aspects of gas-phase fragmentation chemistry are broadly applicable to carbohydrates and which are more structural family-specific. For example, which structural and energetic constraints are imposed by the glycosidic bond linkage stereochemistry ( $\alpha/\beta$ ) and positions? The long-term hope is to apply this into a practically useful algorithm for computational prediction of glycan sequence. This would complement existing methods of glycan identification. Finally we should note that unfortunately there is very little other computational data available to which we can compare our findings [14, 19, 37, 38]. Additionally, much of this is concerned with the very interesting and useful but not commonly available technique,

electronic excitation dissociation [14, 19], so it cannot be directly compared to the present experimental conditions. Subsequent work from our laboratory and others should overcome this deficiency.

## Acknowledgments

The authors acknowledge support for this work by start-up funds from the University of Missouri-St. Louis and a University of Missouri Research Board Grant. Calculations were performed at the Missouri University of Science and Technology, Rolla, MO. M.T.A. thanks the Saudi Arabia Culture Mission for a graduate fellowship.

## References

1. Vanderschaeghe, D., Festjens, N., Delanghe, J., Callewaert, N.: Glycome profiling using modern glycomics technology: technical aspects and applications. *Biol. Chem.* **391**, 149–161 (2010)
2. Hart, G.W., Copeland, R.J.: Glycomics hits the big time. *Cell* **143**, 672–676 (2010)
3. Varki, A., Cummings, R.D., Esko, J.D., Freeze, H.H., Stanley, P., Betozzi, C.R., Hart, G.W., Etzler, M.E.: *Essentials of Glycobiology*, Cold Spring Harbor Laboratory Press, New York (2008)
4. An, H.J., Kronewitter, S.R., De Leoz, M.L.A., Lebrilla, C.B.: Glycomics and disease markers. *Curr. Opin. Chem. Biol.* **13**, 601–607 (2010)
5. Petrescu, A.J., Wormald, M.R., Dwek, R.A.: Structural aspects of glycomes with a focus on M-glycosylation and glycoprotein folding. *Curr. Opin. Struct. Biol.* **16**, 600–607 (2006)
6. Dalziel, M., Crispin, M., Scanlan, C.N., Zitzmann, N., Dwek, R.A.: Emerging principles for the therapeutic exploitation of glycosylation. *Science* **343**, 1235681 (2014)
7. Alley Jr., W.R., Novotny, M.V.: Structural glycomics analyses at high sensitivity: a decade of progress. *Annu. Rev. Anal. Chem.* **6**, 237–265 (2013)
8. Scanlan, C.N., Offer, J., Zitzmann, N., Dwek, R.A.: Exploiting defensive sugars of HIV-1 for drug and vaccine design. *Nature* **446**, 1038–1045 (2007)
9. Domon, B., Costello, C.E.: A systematic nomenclature for carbohydrate fragmentations in FAB-MS/MS spectra of glycoconjugates. *Glycoconj. J.* **5**, 397–409 (1988)
10. Zaia, J.: Mass spectrometry of oligosaccharides. *Mass Spectrom. Rev.* **23**, 161–227 (2004)
11. An, H.J., Froehlich, J.W., Lebrilla, C.B.: Determination of glycosylation sites and site-specific heterogeneity in glycoproteins. *Curr. Opin. Chem. Biol.* **13**, 421–426 (2010)
12. Park, Y., Lebrilla, C.B.: Application of Fourier transform ion cyclotron resonance mass spectrometry to oligosaccharides. *Mass Spectrom. Rev.* **24**, 232–264 (2005)
13. Kailemia, M.J., Ruhaak, L.R., Lebrilla, C.B., Amster, I.J.: Oligosaccharide analysis by mass spectrometry: a review of recent developments. *Anal. Chem.* **86**, 196–212 (2013)
14. Yu, X., Jiang, Y., Huang, Y., Costello, C.E., Lin, C.: Detailed glycan structural characterization by electronic excitation dissociation. *Anal. Chem.* **85**, 10017–10021 (2013)
15. Cancilla, M.T., Penn, S.G., Lebrilla, C.B.: Alkaline degradation of oligosaccharides coupled with matrix-assisted laser desorption/ionization Fourier transform mass spectrometry: a method for sequencing oligosaccharides. *Anal. Chem.* **70**, 663–672 (1998)
16. Orlando, R., Bush, C.A., Fenselau, C.: Structural analysis of oligosaccharides by tandem mass spectrometry: collisional activation of sodium adduct ions. *Biomed. Environ. Mass Spectrom.* **19**, 747–754 (1990)
17. Hofmeister, G.E., Zhou, Z., Leary, J.A.: Linkage position determination in lithium-cationized disaccharides: tandem mass spectrometry and semi-empirical calculations. *J. Am. Chem. Soc.* **113**, 5964–5970 (1991)

18. Reinhold, V.N., Reinhold, B.B., Costello, C.E.: Carbohydrate molecular weight profiling, sequence, linkage, and branching data: ES-MS and CID. *Anal. Chem.* **67**, 1772–1784 (1995)
19. Huang, Y., Pu, Y., Yu, X., Costello, C.E., Lin, C.: Mechanistic study on electronic excitation dissociation of the cellobiose–Na<sup>+</sup> complex. *J. Am. Soc. Mass Spectrom.* **27**, 319–328 (2016)
20. Hu, H., Huang, Y., Mao, Y., Yu, X., Xu, Y., Liu, J., Zong, C., Boons, G.-J., Lin, C., Xia, Y., Zaia, J.: A computational framework for heparan sulfate sequencing using high-resolution tandem mass spectra. *Mol. Cell. Proteomics* **13**, 2490–2502 (2014)
21. Yu, X., Huang, Y., Lin, C., Costello, C.E.: Energy-dependent electron activated dissociation of metal-adducted permethylated oligosaccharides. *Anal. Chem.* **84**, 7487–7494 (2012)
22. Fentabil, M.A., Daneshfar, R., Kitova, E.N., Klassen, J.S.: Blackbody infrared radiative dissociation of protonated oligosaccharides. *J. Am. Soc. Mass Spectrom.* **22**, 2171–2178 (2011)
23. Asam, M.R., Glish, G.L.: Tandem mass spectrometry of alkali cationized polysaccharides in a quadrupole ion trap. *J. Am. Soc. Mass Spectrom.* **8**, 987–995 (1997)
24. Harvey, D.J.: Identification of protein-bound carbohydrates by mass spectrometry. *Proteomics* **1**, 311–328 (2001)
25. Harvey, D.J.: Matrix-assisted laser desorption/ionization mass spectrometry of carbohydrates. *Mass Spectrom. Rev.* **18**, 349–451 (1999)
26. Harvey, D.J., Bateman, R.H., Green, M.R.: High-energy collision-induced fragmentation of complex oligosaccharides ionized by matrix-assisted laser desorption/ionization mass spectrometry. *J. Mass Spectrom.* **32**, 167–187 (1997)
27. Ashline, D.J., Lapadula, A.J., Liu, Y.-H., Lin, M., Grace, M., Pramanik, B., Reinhold, V.N.: Carbohydrate structural isomers analyzed by sequential mass spectrometry. **79**, 3830–3842 (2007)
28. Huang, Y., Dodds, E.D.: Ion mobility studies of carbohydrates as group I adducts: isomer specific collision cross section dependence on metal ion radius. *Anal. Chem.* **85**, 9728–9735 (2013)
29. Huang, Y., Dodds, E.D.: Discrimination of isomeric carbohydrates as the electron transfer products of group II cation adducts by ion mobility mass spectrometry and tandem mass spectrometry. *Anal. Chem.* **87**, 5664–5668 (2015)
30. Gaye, M.M., Kurulugama, R., Clemmer, D.E.: Investigating carbohydrate isomers by IMS-CID-IMS-MS: precursor and fragment ion cross-sections. *Analyst* **140**, 6922–6932 (2015)
31. Hoffmann, W., Hofmann, J., Pagel, K.: Energy-resolved ion mobility-mass spectrometry—a concept to improve the separation of isomeric carbohydrates. *J. Am. Soc. Mass Spectrom.* **25**, 471–479 (2013)
32. Zhu, F., Glover, M.S., Trinidad, J.C., Clemmer, D.E.: Populations of metal-glycan structures influence MS fragmentation patterns. *J. Am. Soc. Mass Spectrom.* **26**, 25–35 (2015)
33. Zhu, M., Bendiak, B., Clowers, B., Hill, H.H.: Ion mobility-mass spectrometry analysis of isomeric carbohydrate precursor ions. *Anal. Bioanal. Chem.* **394**, 1853–1867 (2009)
34. Pagel, K., Harvey, D.J.: Ion mobility-mass spectrometry of complex carbohydrates: collision cross-sections of sodiated N-linked glycans. *Anal. Chem.* **85**, 5138–5145 (2013)
35. Cancilla, M.T., Penn, S.G., Carroll, J.A., Lebrilla, C.B.: Coordination of alkali metals to oligosaccharides dictates fragmentation behavior in matrix assisted laser desorption ionization/Fourier transform mass spectrometry. *J. Am. Chem. Soc.* **118**, 6736–6745 (1996)
36. Spengler, B., Dolce, J.W., Cotter, R.J.: Infrared laser desorption mass spectrometry of oligosaccharides: fragmentation mechanisms and isomer analysis. *Anal. Chem.* **62**, 1721–1737 (1990)
37. Suzuki, H., Kameyama, A., Tachibana, K., Narimatsu, H., Fukui, K.: Computationally and experimentally derived general rules for fragmentation of various glycosyl bonds in sodium adduct oligosaccharides. *Anal. Chem.* **81**, 1108–1120 (2009)
38. Yamagaki, T., Fukui, K., Tachibana, K.: Analysis of glycosyl bond cleavage and related isotope effects in collision-induced dissociation quadrupole-time-of-flight mass spectrometry of isomeric trehaloses. *Anal. Chem.* **78**, 1015–1022 (2006)
39. Frisch, M. J., Trucks, G. W., Schlegel, H. B., Scuseria, G. E., Robb, M. A., Cheeseman, J.R., Scalmani, G., Barone, V., Mennucci, B., Petersson, G. A., Nakatsuji, H., Caricato, M., Li, X., Hratchian, H. P., Izmaylov, A. F., Bloino, J., Zheng, G., Sonnenberg, J. L., Hada, M., Ehara, M., Toyota, K., Fukuda, R., Hasegawa, J., Ishida, M., Nakajima, T., Honda, Y., Kitao, O., Nakai, H., Vreven, T., Montgomery, J. A., Jr., Peralta, J. E., Ogliaro, F., Bearpark, M., Heyd, J.J., Brothers, E., Kudin, K. N., Staroverov, V. N., Kobayashi, R., Normand, J., Raghavachari, K., Rendell, A., Burant, J. C., Iyengar, S. S., Tomasi, J., Cossi, M., Rega, N., Millam, J. M., Klene, M., Knox, J. E., Cross, J. B., Bakken, V., Adamo, C., Jaramillo, J., Gomperts, R., Stratmann, R.E., Yazyev, O., Austin, A. J., Cammi, R., Pomelli, C., Ochterski, J. W., Martin, R. L., Morokuma, K., Zakrzewski, V. G., Voth, G. A., Salvador, P., Dannenberg, J. J., Dapprich, S., Daniels, A. D., Farkas, Ö., Foresman, J. B., Ortiz, J. V., Cioslowski, J., Fox, D. J. *Gaussian 09*, Revision B.01, Gaussian, Inc., Wallingford CT, 2009.
40. Zhao, Y., Schultz, N.E., Truhlar, D.G.: Exchange-correlation functional with broad accuracy for metallic and nonmetallic compounds, kinetics, and noncovalent interactions. *J. Chem. Phys.* **123**(16), 161103 (2005)
41. Zhao, Y., Truhlar, D.G.: The M06 suite of density functionals for main group thermochemistry, thermochemical kinetics, noncovalent interactions, excited states, and transition elements: two new functionals and systematic testing of four M06-class functionals and 12 other functionals. *Theor. Chem. Accounts* **120**, 215 (2006)
42. Nelson, C.R., Abutokaikah, M.T., Harrison, A.G., Bythell, B.J.: Proton mobility in b2 ion formation and fragmentation reactions of histidine-containing peptides. *J. Am. Soc. Mass Spectrom.* **27**, 487–497 (2016)
43. Abutokaikah, M.T., Guan, S., Bythell, B.J.: Stereochemical sequence ion selectivity: proline versus pipecolic acid-containing protonated peptides. *J. Am. Soc. Mass Spectrom.* (2016).doi:10.1007/s13361-016-1510-1
44. Hernandez, O., Isenberg, S., Steinmetz, V., Glish, G.L., Maitre, P.: Probing mobility selected saccharide isomers: selective ion-molecule reactions and wavelength-specific IR activation. *J. Phys. Chem. A* **119**, 6057–6064 (2015)
45. Ngoka, L.C., Gal, J.-F., Lebrilla, C.B.: Effects of cations and charge types on the metastable decay rates of oligosaccharides. *Anal. Chem.* **66**, 692–698 (1994)
46. Fenn, L.S., McLean, J.A.: Structural resolution of carbohydrate positional and structural isomers based on gas-phase ion mobility-mass spectrometry. *J. Phys. Chem. Phys.* **13**, 2196–2205 (2011)
47. Jones, J.L., Dongre, A.R., Somogyi, A., Wysocki, V.H.: Sequence dependence of peptide fragmentation efficiency curves determined by electrospray ionization/surface-induced dissociation mass spectrometry. *J. Am. Chem. Soc.* **116**, 8368–8369 (1994)
48. Somogyi, A., Wysocki, V.H., Mayer, I.: The effect of protonation site on bond strengths in simple peptides: application of ab initio and modified neglect of differential overlap bond orders and modified neglect of differential overlap energy partitioning. *J. Am. Soc. Mass Spectrom.* **5**, 704–717 (1994)
49. Bythell, B.J., Suhai, S., Somogyi, A., Paizs, B.: Proton-driven amide bond-cleavage pathways of gas-phase peptide ions lacking mobile protons. *J. Am. Chem. Soc.* **131**, 14057–14065 (2009)
50. El Aribi, H., Orlova, G., Rodriguez, C.F., Almeida, D.R.P., Hopkinson, A.C., Siu, K.W.M.: Fragmentation mechanisms of product ions from protonated tripeptides. *J. Phys. Chem. B* **108**, 18743–18749 (2004)
51. El Aribi, H., Rodriguez, C.F., Almeida, D.R.P., Ling, Y., Mak, W.W.N., Hopkinson, A.C., Siu, K.W.M.: Elucidation of fragmentation mechanisms of protonated peptide ions and their products: a case study on glycylglycylglycine using density functional theory and threshold collision-induced dissociation. *J. Am. Chem. Soc.* **125**, 9229–9236 (2003)
52. Paizs, B., Suhai, S.: Fragmentation pathways of protonated peptides. *Mass Spectrom. Rev.* **24**, 508–548 (2005)
53. Rodriguez, C.F., Cunje, A., Shoeib, T., Chu, I.K., Hopkinson, A.C., Siu, K.W.M.: Proton migration and tautomerism in protonated triglycine. *J. Am. Chem. Soc.* **123**, 3006–3012 (2001)
54. Wysocki, V.H., Tsapralis, G., Smith, L.L., Brechi, L.A.: Mobile and localized protons: a framework for understanding peptide dissociation. *J. Mass Spectrom.* **35**, 1399–1406 (2000)
55. Feng, S., Bagia, C., Mpourmpakis, G.: Determination of proton affinities and acidity constants of sugars. *J. Phys. Chem. A* **117**, 5211–5219 (2013)
56. Harrison, A.G.: Linear free energy correlations in mass spectrometry. *J. Mass Spectrom.* **34**, 577–589 (1999)
57. Jawad, R., Elleman, C., Vermeer, L.S., Drake, A.F., Woodhead, B., Martin, G.P., Royall, P.G.: Measurement of the  $\beta/\alpha$  anomer composition within amorphous lactose prepared by spray and freeze drying using a simple <sup>1</sup>H-NMR method. *Pharm. Res.* **29**, 511–524 (2011)
58. Paizs, B., Suhai, S.: Towards understanding the tandem mass spectra of protonated oligopeptides. 1: mechanism of amide bond cleavage. *J. Am. Soc. Mass Spectrom.* **15**, 103–113 (2004)

59. Heaton, A.L., Armentrout, P.B.: Experimental and theoretical studies of sodium cation interactions with d-arabinose, xylose, glucose, and galactose. *J. Phys. Chem. A* **112**, 10156–10167 (2008)
60. Bythell, B.J., Dain, R.P., Curtice, S.S., Oomens, J., Steill, J.D., Groenewold, G.S., Paizs, B., Van Stipdonk, M.J.: Structure of  $[M + H - H_2O]^+$  from protonated tetraglycine revealed by tandem mass spectrometry and IRMPD spectroscopy. *J. Phys. Chem. A* **114**, 5076–5082 (2010)
61. Verkerk, U.H., Zhao, J., Van Stipdonk, M.J., Bythell, B.J., Oomens, J., Hopkinson, A.C., Siu, K.W.M.: Structure of the  $[M + H - H_2O]^+$  Ion from tetraglycine: a revisit by means of density functional theory and isotope labeling. *J. Phys. Chem. A* **115**, 6683–6687 (2011)
62. Bythell, B.J., Harrison, A.G.: Formation of  $a_1$  ions directly from oxazolone  $b_2$  ions: an energy-resolved and computational study. *J. Am. Soc. Mass Spectrom.* **26**, 774–781 (2015)
63. Gritsenko, O.V., Ensing, B., Schipper, P.R.T., Baerends, E.J.: Comparison of the accurate Kohn-Sham solution with the generalized gradient approximations (GGAs) for the SN2 Reaction  $F^- + CH_3F \rightarrow FCH_3 + F^-$ : a qualitative rule to predict success or failure of GGAs. *J. Phys. Chem. A* **104**, 8558–8565 (2000)
64. Bleiholder, C., Paizs, B.: Competing gas-phase fragmentation pathways of asparagine-, glutamine-, and lysine-containing protonated dipeptides. *Theor. Chem. Accounts* **125**, 387–396 (2010)
65. Bythell, B.J., Barofsky, D.F., Pingitore, F., Polce, M.J., Wang, P., Wesdemiotis, C., Paizs, B.: Backbone cleavages and sequential loss of carbon monoxide and ammonia from protonated AGG: a combined tandem mass spectrometry, isotope labeling, and theoretical study. *J. Am. Soc. Mass Spectrom.* **18**, 1291–1303 (2007)
66. Laerdahl, J.K., Uggerud, E.: Gas-phase nucleophilic substitution. *Int. J. Mass Spectrom.* **214**, 277–314 (2002)